Lithium Powder Synthesis and Preparation of Powder-Based Composite Electrodes for Application in Lithium Metal Batteries

Aleksei Kolesnikov, Tristan Wulfers, Martin Kolek, Peter Bieker, Marian Cristian Stan, and Martin Winter**

The electrochemical performance of lithium metal batteries is affected by many factors, among which the negative electrode is crucial. Although much of the research is focused on lithium metal electrodes from metallic foils, lithium metal powder can also provide several advantages. Herein, the synthesis of lithium metal powder (Li_p) using a droplet emulsion technique is described in detail and the scientific background of the method is provided. Furthermore, the electrochemical performance of the composite Li_p-based electrodes prepared with conductive carbon additive (Super C65) via the electrode paste-casting method is reported. The results indicate that under the same material loading, the composite Li_p-based electrodes can provide at least twice the practical electrode capacity of pure Li_p electrodes and with lower overpotentials, as shown in symmetric Li||Li cells. Full cells assembled with an NMC622 cathode and a composite Li_p-based electrode are cycled at least for 100 cycles and show improved cycling performance as compared with the full cells assembled with pure Li_p electrodes. In addition, the results also conclude that there are four different types of charge storage mechanisms in these composite Li_p-based electrodes. These occurring mechanisms should be considered when engineering lithium metal electrodes with various designs.

1. Introduction

Due to its very favorable cost−performance ratio, the lithium ion battery (LIB) technology, first commercialized in the early 1990s,[1–3] remains the best example of a rechargeable high-energy-density battery that is remodeling our society.

Negative electrodes based on lithium metal (Li) as active material allow a significant increase in the specific energy (Wh kg^{-1}) of rechargeable batteries due to the physicochemical properties of Li such as the low standard reduction potential (–3.04 V versus standard hydrogen electrode) and light weight.[4,5]

To overcome the safety and performance issues during the charge/discharge process related to the formation of heterogeneous Li deposits, the so-called high-surface-area lithium (HSAL[6] or dendrites), and improve the electrochemical performance of rechargeable lithium metal batteries (LMBs), several measures, such as interphase engineering,[7,8] application of 3D current collectors,[9–12] use of "alloying" metals and intermetallics,[12–16] tailoring of electrolyte compositions,[17,18] and use of solid-state electrolytes,[19,20] were considered.

Kim et al.[21] introduced the droplet emulsion technique (DET) for synthesis of lithium powder (Li_p) that was used for the preparation of compact Li_p electrodes. In comparison with Li foil electrodes, the Li_p electrodes demonstrated lower impedance and reduced HSAL formation after Li electrodeposition/electrodissolution processes. The improved performance was attributed to the higher ionic conductivity of the solid−electrolyte interphase (SEI)[22] formed on such Li_p particles and the larger surface area of the Li_p electrodes that lead to lower local current densities and thus suppressed HSAL formation.[21] Based on the work of Kim et al.,[21] further studies focused on the synthesis of surface-coated Li_p,[23] where improved performance of Li_p electrodes was achieved by the application of a higher compression degree,[24] the preparation of composite Li_p electrodes using Cu powder,[25] and by chemical modification of the Li_p particles in Li_p electrodes using a cementation reaction with ZnI_2.[26] Although the DET method was described in regard to the processing steps,[23,27,28] little work has been focused on deciphering the effect that various parameters within the DET method have on the particle size, shape, and interfacial properties of the synthesized Li_p particles.

In this work, we first present in detail the scientific background of the DET method, followed by investigations of

A. Kolesnikov, T. Wulfers, M. Kolek, P. Bieker, M. C. Stan, M. Winter
MEET Battery Research Center
University of Münster
Corrensstrasse 46, 48149 Münster, Germany
E-mail: martin.winter@uni-muenster.de; marian.stan@uni-muenster.de

M. Winter
Helmholtz Institute Münster (HI MS)
IEK-12
Forschungszentrum Jülich GmbH
Corrensstrasse 46, 48149 Münster, Germany

The ORCID identification number(s) for the author(s) of this article can be found under https://doi.org/10.1002/ente.202100871.

DOI: 10.1002/ente.202100871

the synthesized Li_p particles prepared in composite Li_p electrodes using a commonly known electrode paste-casting method. In previous studies, we demonstrated that poor electronic contact at the Li|Li and Cu|Li interfaces in pure Li_p electrodes limits the use of a substantial amount of Li contained in the electrodes and results in poor capacity utilization.[26,29] Carbon black, that is a commercial product consisting of a nearly pure elemental carbon with application in rubber automotive products, plastics, and paints,[30] was used here as a conductive additive especially due to its high electronic conductivity.[31–35] As a candidate for the conductive additive, commonly encountered in LIBs, Super C65 was employed for the preparation of composite Li_p electrodes. Furthermore, the influence of the conductive additive on the electrochemical performance of the resultant composite Li_p electrodes in laboratory coin cells is discussed and four different types of charge storages are described.

2. Experimental Section

Li_p synthesis was performed with the DET using an in-house-built cylindrical container made of stainless steel as the synthesis reactor (**Figure 1**). Tetradecane (VWR, 99%) was used as an inert medium, whereas Li ingots (CEL, battery grade) were used as Li source for Li_p synthesis. In a typical synthesis, 1 g of Li pellets and 150 mL of the inert medium were transferred into the synthesis reactor. Then, the reactor was gradually heated up to 220 °C using a hot plate and kept at this temperature for 5 min. Then, using a DREMEL 4000 stirrer, the inert medium and Li melt were stirred at ≈20 000 rpm for 5 min to produce an emulsion of Li droplets. When the heating was stopped, the reactor cooled down to room temperature and this resulted in the solidification of the Li droplets and formation of Li_p particles. The separation of Li_p particles from the inert medium was carried out by filtration and the resultant Li_p particles were rinsed with *n*-hexane (Sigma Aldrich, anhydrous, 95%) three times to remove residuals of the inert medium. Only the Li_p particles with a diameter ≤100 μm were collected by sieving (mesh size: 0.1 mm) and further used to prepare the composite Li_p electrodes. All processes were carried out in a dry room, where the dew point was −50 °C, except sieving, that was conducted in an argon-filled glovebox (with O_2 and H_2O values lower than 0.1 ppm).

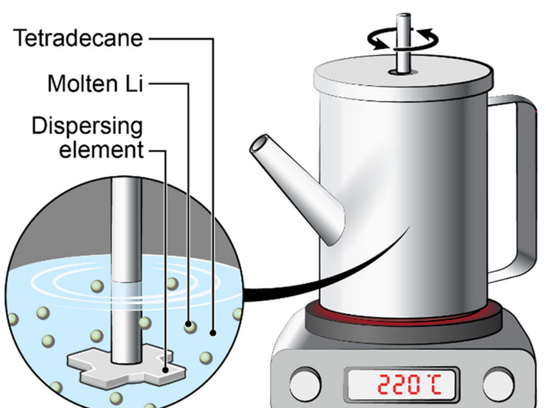

Figure 1. Schematic representation of the synthesis reactor used for the synthesis of the Li_p particles used in this study.

To prepare the pure Li_p electrodes, Li_p was mixed with a solution of 3 wt% of poly(isobutylene) (PIB, Oppanol B200, BASF) in heptane (Sigma Aldrich, anhydrous 99%) and coated on dendritic Cu foil (18 μm, Schlenk Metal Foils GmbH & Co. KG). After drying under reduced pressure at 60 °C for 12 h, the Li_p electrodes with a final composition of 95 wt% Li_p and 5 wt% binder were obtained. These Li_p electrodes were roll pressed to 100 μm (30% compression degree), using a bench-top calendar machine (MTI Corp., MR100DC). The composite Li_p electrodes were prepared using the same procedure as above to the final composition of 90 wt% Li_p, 5 wt% conductive carbon (Super C65, Imerys Graphite & Carbon, surface area 62 $m^2\,g^{-1}$),[36] and 5 wt% binder. Similarly, pure Super C65 (CC) electrodes were prepared with a final composition of 80 wt% CC and 20 wt% PIB. All electrodes were dried under reduced pressure at 60 °C for more than 12 h. The CC electrode thickness after calendering (30% compression degree) was ≈30 μm and the mass loading of the electrode coating (CC and PIB) was ≈0.5 mg cm^{-2}. A reversible specific capacity of CC after the first cycle in a CC||Li cell was experimentally found to be 101 mAh g^{-1}. The positive electrode was prepared using $LiNi_{0.6}Mn_{0.2}Co_{0.2}O_2$ (NMC 622, BASF) as active material and was mixed with a solution of poly(vinylidene difluoride) (PVdF, Solvay) in *N*-methyl-2-pyrrolidone (NMP, anhydrous, 99.5% Sigma-Aldrich) and conductive agent Super C65 using an intensive mixer Labormischer R02 VAC (EIRICH EVACTHERM) to a final composition of 95:2:3 (wt%, active material: conductive agent: binder). The slurry was coated on an aluminum current collector, with a wet film thickness of 120 μm, leading to an average capacity per area subjected to calendaring (electrode porosities of ≈30%) and finally of ≈1.3 mAh cm^{-2}. The electrode sheets were predried at 70 °C and cut into disks (12 mm diameter) prior the final drying step, performed under reduced pressure (10^{-3} mbar) and at 120 °C for 12 h.

The nominal capacity of the Li_p electrodes was determined using two-electrode[37] coin cells (CR2032) and a battery tester Maccor Series 4000 (Maccor Inc.). For this, Cu||Li_p cells assembled with a separator stack including four layers of nonwoven poly(propylene) separator (Freudenberg, FS 2190) one layer of Celgard 2500 separator were used. The separator was soaked with 120 μL of electrolyte and 1 M $LiPF_6$ in EC:DEC 3:7 (w/w) (LP47, BASF SE). The Cu||Li_p cells were discharged using a current density of 0.5 mA cm^{-2} until the cutoff voltage of −1.5 V was reached.

For cycling stability investigations, Li||Li symmetric cells assembled with a Celgard 2500 separator soaked with 30 μL electrolyte (1 M $LiPF_6$ in EC:DEC 3:7 (w/w), BASF SE) were cycled using a current density of 0.5 mA cm^{-2} with cutoff voltages of −1.5 and 1.5 V.

Three-electrode NMC622||Li cells were assembled using Li as reference electrode.[37] The negative and positive electrodes were separated by one layer of Celgard 2500 separator. The separator was soaked with 30 μL of electrolyte. The NMC622||Li cells were charged and discharged at a constant current corresponding to 0.2C rate (charge) and 0.2C rate (discharge) between the potential limits 4.3 and 3.0 V versus Li/Li^+. All the measurements were carried out at 20 °C and all cells were assembled inside a dry room (dew point: −50 °C).

The morphology of the Li_p electrodes was investigated using a scanning electron microscope (SEM, Zeiss Auriga Crossbeam Workstation) with a field-emission gun (Schottky-type) and an energy-dispersive X-ray (EDX) spectroscopy system (X–Max 80 mm^2 detector, Oxford Instruments).

The X-ray diffraction (XRD) pattern of Li_p was collected using AXS Bruker D8 Advance diffractometer (Bruker) with Cu Kα radiation ($\lambda_{Cu} = 0.15418$ nm) and equipped with a Lynx-Eye 1D position-sensitive detector (PSD). The XRD pattern was recorded for $20° \leq 2\theta \leq 80°$ using a step size of 0.02 and a time per step of 0.2 s. To carry out the measurements, the Li_p particles were fixed on the sample holder (single crystal silicon) using a special tape to avoid contact with air and moisture during the measurement.

Electrochemical impedance spectroscopy (EIS) of Li||Li symmetric cells was measured using a Solartron SI 1287 potentiostat/galvanostat in combination with a Solartron SI 1260 impedance/gain phase analyzer. The spectra were recorded in the frequency range of 1 MHz−10 mHz and a voltage amplitude of 5 mV.

3. Results and Discussion

The DET is a well-established method for synthesis of Li_p particles. The method relies on the melting and emulsification of Li metal in a chemically inert liquid medium. Heating of Li metal (in the form of ingots, rods, or foils) above its melting point (180.5 °C) causes a change in the aggregate state of Li metal from solid to liquid and leads to interface formation between the two immiscible liquids. Silicon oil and long-chain saturated hydrocarbons are typically used as a chemically inert liquid media for the synthesis of Li_p due to their chemical stability against Li metal. Whenever the contact of different phases (here: molten Li and inert medium) is established, interfacial phenomena need to be considered. Li atoms inside the Li metal melt phase are surrounded by other Li atoms and the van der Waals forces between them result in an equally distributed attraction. Li atoms at the surface of the Li metal melt phase interact also with molecules of the inert medium, which leads to an imbalance of forces on these Li atoms. As a result of this imbalance, the surface of the Li metal in the melt phase tends to contract spontaneously, which is generally described as surface tension.[38]

Following the Gibbs−Duhem equation (Equation (1)), surface tension is defined as the free energy required to increase the surface of the liquid phase by a unit of surface at constant temperature and composition (Equation (1)).[39]

$$dG^\sigma = -S^\sigma dT + Ad\gamma + \sum n_i d\mu_i \quad (1)$$

where G^σ is the surface Gibbs free energy [J], $S^\sigma dT$ is an entropy term (S^σ: entropy [J K^{-1}] and T: temperature [K]), $Ad\gamma$ is interfacial energy term (A is the surface area [m^2] and γ is the surface tension [J m^{-2} or N m^{-1}]), and $\sum n_i d\mu_i$ is composition term (n_i is the number of moles of component i with the chemical potential μ_i [J mol^{-1}]).

At constant temperature and composition, the following equations are valid.

$$dG^\sigma = Ad\gamma \quad (2)$$

$$\gamma = \left(\frac{\partial G^\sigma}{\partial A}\right)_{T,n_i} \quad (3)$$

Thus, a system with a smaller interfacial area ("system state 1"), as it is the case of larger Li metal droplets, will have a smaller Gibbs free energy in comparison with the system where the interfacial area is larger ("system state 2"), as it is the case with smaller Li metal droplets. Hence, to increase the interfacial area of the emulsion, that is, to produce smaller Li metal droplets, an energy amount that is equal to the change in the Gibbs free energy between "system state 1" and "system state 2" needs to be added to the system.[40]

In the current embodiment of the DET, the required energy was provided to the system through vigorous stirring. Shear stress generated in the system acts at the interface between the Li metal droplets and the inert medium that results in deformation of the larger Li droplets with the subsequent break up into smaller droplets. The velocity of this process is determined by fluid dynamics. In a laminar flow, when fluids flow in parallel layers without lateral mixing, the generated shear stress is lower. Accordingly, the emulsion formation is slower in comparison with turbulent flow characterized by chaotic fluid movement. To predict the flow type, Reynolds number (Re) can be applied, which is calculated based on fluid properties and apparatus parameters. The fluid flow in a system is defined as turbulent at Re >2000.[39]

For the mechanically agitated vessel used in this study, the Reynolds number was calculated according to Equation (4).[41]

$$Re = \frac{Nd^2\rho}{\mu} \quad (4)$$

where ρ is the density (kg m^{-3}), μ is the viscosity (kg $(m\,s)^{-1}$), N is the number of rotations per second (rot s^{-1}), and d is the maximum diameter of the impeller rotor (m).

For calculation, the following values were considered: density[42] of tetradecane $\rho = 761$ kg m^{-3}, viscosity[43] of tetradecane $\mu = 2.08$ mPa s, maximum diameter of the impeller rotor $d = 0.02$ m, and stirring speed $N = 20\,000$ rpm $= 333$ rot s^{-1}. The calculated value $Re = 47\,782$ indicates a turbulent flow during the synthesis of Li_p.

In the last step of DET-based synthesis, the emulsion is cooled down to room temperature that results in solidification of Li metal droplets, that is, Li_p particle formation, when the temperature decreases below the melting point of Li metal. The SEM image of the synthesized Li_p (**Figure 2**a) demonstrates spherical particles with an average size ≤100 μm. The presence of Li in the synthesized Li_p was confirmed by XRD and the pattern, assigned to Li metal (PDF 01-071-5949), is presented in Figure 2b. Due to the high reactivity of molten Li, it can easily react with gaseous or dissolved species (e.g., O_2, CO_2, H_2O) in the inert medium that would result in the formation of a native surface film on Li_p particles containing Li species such as Li_2CO_3, Li_2O, and LiOH. The extent of various side reactions reduces finally the amount of "active" Li contained in the Li_p particles and subsequently, also reduces the practical capacity of the resultant Li_p electrodes. In previous reports, we demonstrated that only a limited amount of

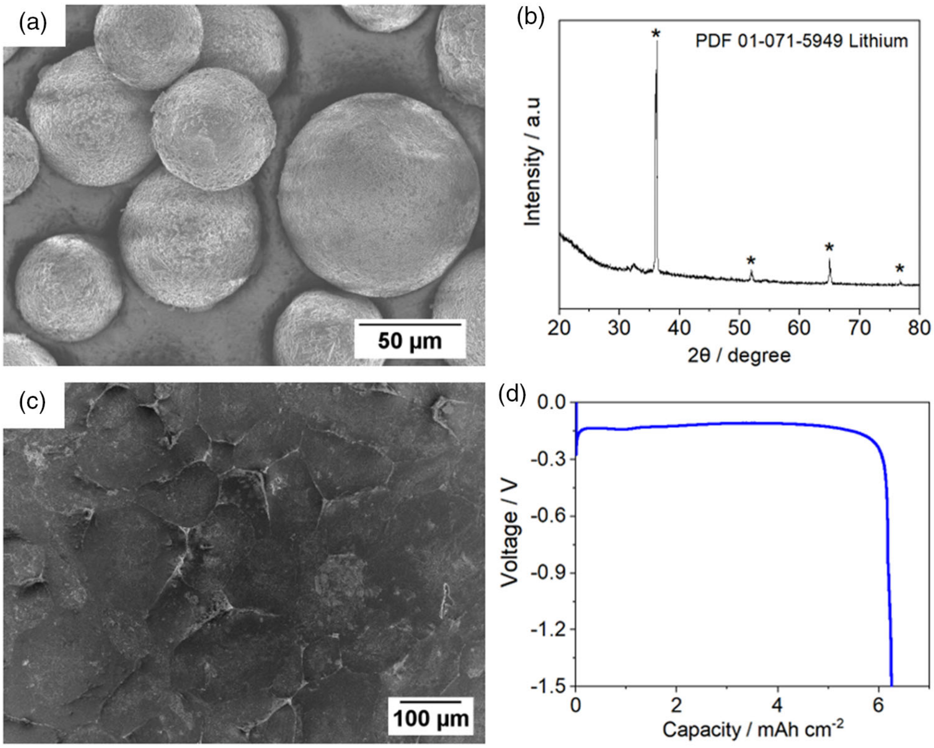

Figure 2. Typical a) SEM image and b) XRD pattern of the synthesized Li_p particles. c) SEM image of pure Li_p electrodes after being compressed. d) Practical electrode capacity determined in Cu||Li cells using 1 M $LiPF_6$ in EC:DEC 3:7 (w/w) as electrolyte and a current density of 0.5 mA cm^{-2}.

Li, contained in Li_p electrodes, can be used for the Li electrodissolution/electrodeposition process due to the poor conductivity in the composite electrode and corrosion-related processes.[26,29]

To counteract the poor conductivity and the interparticle contact in the pure Li_p electrodes and thus, to better determine the total amount of electrochemically active Li in Li_p electrodes, a high compression degree (≈70%) was applied during calendaring of the pure Li_p electrodes.

A high compression degree leads to the loss of the original powder morphology, as the spherical particles are crushed under high pressure, and results in a Li metal foil-like structure. However, boundaries, remaining from the individual Li_p particles, can still be observed in such highly compressed (HC) Li_p electrodes (Figure 2c). Such HC-Li_p electrodes are well suited for determination of the amount of electrochemically active Li in Li_p electrodes, as the negative effects, such as, poor electronic conductivity and galvanic corrosion, that are observed for the Li_p electrodes with mostly spherical structures, are reduced in this case. The electronic conductivity is improved as Li forms a continuous phase on the current collector, the surface film covering each individual Li_p particle is broken, and, in contrast to the pure Li_p electrodes, the individual Li_p particles remain in electronic contact with the current collector. As Li forms a continuous phase, the electrolyte cannot penetrate anymore to the current collector and thus the formation of a galvanic element, that is, intimate contact between Cu and Li while being immersed in the electrolyte, is prevented.

The total amount of electrochemically active Li in Li_p electrodes was determined by measuring the practical electrode capacity of the HC Li_p electrodes in Cu||Li_p cells. Figure 2d presents the voltage profile of the Cu||Li_p cell during Li electrodissolution from the HC Li_p electrode and simultaneous Li electrodeposition on the Cu foil using a constant current density of 0.5 mA cm^{-2} until the voltage cutoff value of −1.5 V is reached. Based on this measurement, the HC Li_p electrode delivered a capacity of 6.3 mAh cm^{-2}, which is much higher than that of conventional, uncompressed Li_p electrodes (<2.5 mAh cm^{-2}) reported previously.[26,29] During Li electrodissolution process, some clusters of Li_p particles can be isolated from a current collector, which results in the formation of electrochemically inactive, "dead" Li and leads to the reduced electrode capacity. As mentioned, the HC Li_p electrodes have a Li foil-like structure without individual Li_p particles that prevents loss of electronic contact between the current collector and Li_p particles and, accordingly, results in the increased practical electrode capacity. However, the application of the high compression degrees during calendering of Li_p electrodes can be utilized as a perspective method for production of ultrathin (<20 µm) Li metal electrodes that will be the focus of a perspective study.

For further investigations, pure Li_p electrodes and composite Li_p electrodes (Li_pCC), with a ratio of Li_p:CC = 95:5 (w/w), were used. During calendering, a moderate compression degree of 30% was applied, that allows to reduce the electrode porosity and improve interparticle contact, but preserves the powder-like structure of the electrodes. **Figure 3**a,b shows SEM top-view

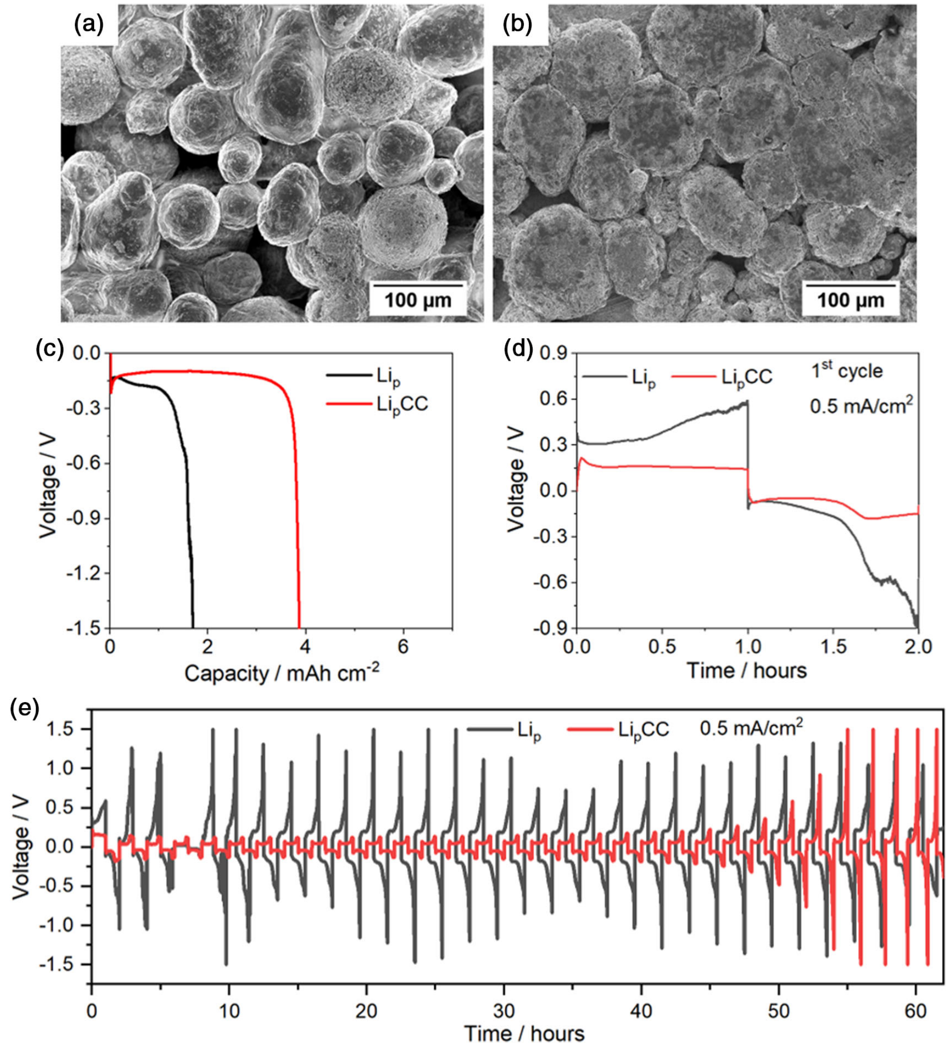

Figure 3. Surface morphology of the Li_p-based electrodes prepared with a) pure Li_p particles and b) composite Li_pCC composite. c) Practical electrode capacity determination in Cu||Li cells. d) Long-term cycling in Li||Li symmetric cells performed in 1 M $LiPF_6$ in EC:DEC 3:7 (w/w) at a current density of 0.5 mA cm^{-2}. e) Voltage profiles of the first cycle in Li||Li symmetric cells.

images of the prepared electrodes. On the surface of the pristine (Figure 3a) and composite electrodes (Figure 3b), individual Li_p particles can be distinguished representing the preservation of powder morphology. Furthermore, the results of SEM/EDX analysis of Li_pCC electrodes (Figure S1, Supporting Information) highlight the well-distributed conductive carbon network along the electrode surface which additionally covers individual Li_p particles. As a result of the carbon network, an improved contact between the individual Li_p particles can be assured. However, it should be mentioned that the rough surface of the Li_p particles, observed in these electrodes, is also a result of the extensive wet electrode preparation procedure and the use of nanometer-sized conductive agent particles.

The practical capacities and the voltage profiles of pure Li_p and composite Li_pCC electrodes shown in Figure 3c indicate that both the capacity utilization as well as the overpotential evolution are superior for the composite electrodes. An enhanced capacity of ≈3.9 mAh cm^{-2} was obtained for the Li_pCC electrode, while only ≈1.8 mAh cm^{-2} was obtained for the pure Li_p electrode. These findings imply that CC significantly improves the contact between Li_p particles and thus, the composite electrode preparation method can be applied to achieve higher practical electrode capacities, while allowing to preserve powder morphology of the Li_p particles.

The cycling stability of pure Li_p and composite Li_pCC electrodes was investigated in Li||Li-symmetric cells using a current density of 0.5 mA cm^{-2} and voltage cutoff value of ±1.5 V. The voltage profiles are presented in Figure 3d for the initial cycle. Pure Li_p electrodes demonstrate high overvoltages during Li electrodeposition/dissolution until the cutoff voltage value of ±1.5 V is reached. In contrast, the composite Li_pCC electrodes showed much lower overvoltage for the Li electrodissolution process (0.16 V) in comparison with that of the pure Li_p electrodes (0.34 V). Such low overvoltages are maintained for several cycles, prior the amount of Li available is depleted (Figure 3e). Further, the observed lower overvoltage of the Li_pCC electrodes also indicates improved kinetics of the electrochemical reaction, that is also in agreement with the EIS data shown in Figure S2, Supporting Information, demonstrating a charge transfer resistance of 43 Ohm for the pure Li_p electrodes (Figure S2a, Supporting Information) and of 7 Ohm for the composite Li_pCC electrodes (Figure S2b, Supporting Information).

The noteworthy difference in the overvoltage after the first cycle indicates changes in Li electrodeposition/electrodissolution behavior. Several studies reported essential influence of a local electric field at an electrode surface on a Li electrodeposition behavior.[44–47] Ding et al.[46] achieved dendrite-free Li electrodeposition utilizing low concentrations of Rb^+ and Cs^+ as electrolyte additives. The ions were electrostatically attracted to Li protuberances (having an enhanced negative charge density), thus changing a local electric field and repelling Li^+ that, in turn, prevented further growth of Li protuberances.[46] Yang et al.[47] prepared a 3D Cu foil with numerous protuberant tips which ensured roughly uniform electric field at the electrode surface serving as charge centers and nucleation sites for Li^+ that resulted in dendrite-free Li electrodeposition. In the Li_pCC electrodes, homogeneously distributed CC, probably, plays a similar role as the protuberant tips do in the 3D Cu foil, that is, ensures uniform electric field in the electrode bulk providing numerous nucleation sites for Li^+. This statement could explain the lower overvoltage observed (after the first cycle in Li||Li symmetric cells) for Li_pCC electrodes (0.15 V/−0.05 V) in comparison with that of Li_p electrodes (0.4 V/−0.13 V) (Figure 3e). Moreover, similar to graphite, CC could serve as a host for Li^+ that also would change Li electrodeposition/electrodissolution behavior for the composite Li_pCC electrodes.

To further clarify a role of CC in composite Li_pCC electrodes, CC electrodes (**Figure** 4a) containing 80 wt.% of CC and 20 wt.% of PIB were prepared and their specific capacity (based on the amount of conducting agent) was determined in CC||Li cells. During this process, Li was transferred from a Li foil electrode to a CC electrode at a current density of 0.1 mA cm^{-2} until the cutoff value of 0 V was reached. After a rest step (open circuit voltage (OCV)) of 3 h, Li was transferred back from the CC electrode to the Li electrode. To maintain consistency with the following experiments, the Li electrodissolution process at the Li foil is referred additionally as the charge process, while the Li electrodeposition at the Li foil is referred to as the discharge process. The voltage profiles of the first cycle (CC||Li cell) are shown in Figure 4b.

Based on the amount of conductive carbon in these electrodes, the calculated specific capacity during the first charge process resulted in almost 197 mAh g^{-1} until the lower cutoff voltage was reached. Also, the voltage profile indicates the presence of several reactions occurring in these electrodes within the investigated voltage range. Considering the electrolyte stability window of liquid−carbonate electrolytes, which are considered to be stable in a voltage range from ≈1.1 to ≈4.5 V (vs. Li | Li^+),[48] side reactions involving the electrolyte within the charge process are not excluded. These reactions, that is, electrolyte decomposition and SEI formation on the surface of the Super C65 particles, can be assigned to the sloping part and the plateau of the voltage profile observed within the voltage range from 0.9 to ≈0.5 V and the plateau at ≈0.5 V. Based on the Super C65 loading in these electrodes, an amount of 100 mAh g^{-1} capacity was delivered within this stage. After that, the cell voltage decreased continuously to the cutoff value of 0 V and a total capacity value of 197 mAh g^{-1} was reached. Therefore, within the first cycle, reactions observed in the voltage profile can be attributed to electrolyte decomposition and SEI formation due to the reasons that 1) liquid−carbonate electrolytes are not stable in this voltage range; and 2) voltage plateaus corresponding to Li^+ intercalation into graphite are typically observed at ≈210, ≈160, ≈130, and ≈80 mV (vs. Li | Li^+).[49] Furthermore, the sloping part of the voltage profile below 0.5 V was attributed to Li^+ insertion into the existing graphite-like domains contained within the CC structure. During the discharge process, the voltage increased continuously to the cutoff value of 1.5 V (vs. Li|Li^+), resulting in reversible specific capacity of 101 mAh g^{-1}. These values are then in accordance with the discussion made above that most of the capacity during the charge process results from side reactions such as electrolyte decomposition and SEI formation. In a separate experiment, the Li electrodeposition on CC electrode was studied in another CC||Li cell. Results are described in detail in supporting information. For this, a Li amount equivalent to 1 mAh cm^{-2} was electrodeposited on CC electrode. SEM images of the CC electrode after Li electrodeposition (Figure S3, Supporting Information) reveal that Li electrodeposition occurs on the surface of both, CC and Cu current collector.

Consequently, the reversible Li^+ insertion into CC and Li electrodeposition on CC imply the existence of different

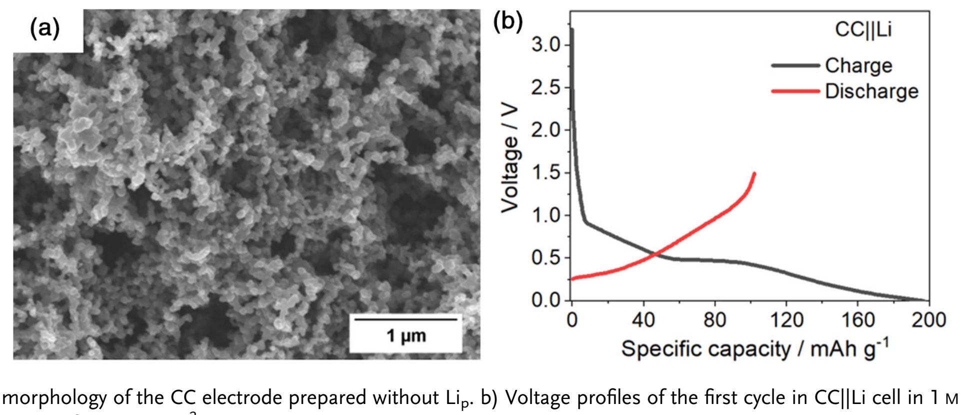

Figure 4. a) Surface morphology of the CC electrode prepared without Li_p. b) Voltage profiles of the first cycle in CC||Li cell in 1 M $LiPF_6$ in EC:DEC 3:7 (w/w) at a current density of 0.1 mA cm^{-2}.

mechanisms of charge storage for pure Li_p electrodes and Li_pCC electrodes. As for Li foil electrodes and for "zero excess" Li electrodes (i.e., current collector-based electrodes without Li or graphite layers), charge can be stored in form of Li metal after Li electrodeposition on Li_p particles and Cu current collector. In contrast, for Li_pCC electrodes, a combination of four charge storage mechanisms can be described. The four possible charge storage mechanisms are summarized in the schematic depictions in **Figure 5**.

The first and the second mechanisms, that is, the charge is stored in the form of Li metal after Li electrodeposition on Li_p particles (Figure 5a) and on Cu current collector (Figure 5b), are also the same as for pure Li_p electrodes. Similar to graphite electrodes in LIB, the charge in Li_pCC electrodes is also stored in the form of Li^+ inserted into CC, which is exemplified by the third charge storage mechanism (Figure 5c). Fourth, as a result of the improvement of cycling life of the Li_pCC symmetric cells when compared with the pure Li_p electrodes, a charge storage mechanism based on Li electrodeposition on lithiated CC can be also described (Figure 5d). In addition, it has to be considered that, after lithiation, CC is both, a lithium-ion conductor and electron conductor. This mixed conduction mechanism is favorable for better distribution of lithium cationic and electronic charge distribution within the composite electrode bulk.

Considering the high surface area of CC ($62\,m^2\,g^{-1}$) which leads to an enhanced SEI formation (and more substrate area for Li electrodeposition) and also the fact that Li^+ can be inserted into CC, corrosion of Li_p particles can be expected to occur. For this reason, morphological investigations of Li_pCC electrodes were performed after 7 days of aging under OCV and results are presented in **Figure 6**.

From the SEM image of an aged composite Li_pCC electrode (Figure 6a), no significant morphological differences can be observed as compared with the pristine composite electrodes. The fact that the CC covers the Li_p particles could, however, cover any signs of galvanic corrosion process. Nevertheless, individual Li_p particles demonstrating signs of corrosion could be identified (Figure 6b–d), revealing the existence of such a galvanic corrosion process[29,50,51] also within the composite Li_pCC electrodes under OCV conditions. Being in intimate contact with both, Li and the electrolyte, CC allows an electron transfer from Li to the electrolyte. As a result, Li is oxidized and dissolved in electrolyte, which leads to morphology changes of the Li_p particles (Figure 6b–d). As a counter reaction to Li oxidation, electrolyte reduction occurs on the surface of CC, resulting in SEI formation. Furthermore, reversible Li^+ insertion into CC, probably, contributes to the morphology changes of Li_p particles, as a mass transport from Li_p particles will result in void formation[50] or hollowed Li_p particles.

The electrochemical behavior of the prepared Li_p-based electrodes was investigated in full cells, using NMC 622 as the cathode material and Li as the reference electrode, at a charge/discharge rate of 0.2C. Furthermore, auxiliary inputs of the battery tester were used to monitor individual potentials of both negative and positive electrodes (vs. the Li reference electrode). The results are presented in **Figure 7** and Figure S4, Supporting Information, showing specific discharge capacities (Figure 7a) and individual potential profiles of the negative (Figure 7c,d) and positive (Figure S4, Supporting Information) electrodes. The specific discharge capacity of the NMC||Li_p cells (Figure 7a) decreases rapidly, within six cycles, from 161 to $120\,mAh\,g^{-1}$, indicating quick consumption of electrochemically active material.[52] In further cycles the specific discharge capacity continuously decreases in a rather noisy fashion and finally drops to zero in the 97th cycle. In contrast, NMC||Li_pCC cells show a stable cycling behavior for at least 100 cycles, with a remaining capacity of $88\,mAh\,g^{-1}$. Such observation is in accordance with the previously reported findings for the Li_pCC symmetric cells (Figure 3e), which indicated that the performance of composite Li_pCC electrodes is superior to that of pure Li_p electrodes. The Coulombic efficiency (Figure 7b) also indicates a rather scattering behavior for the NMC||Li_p cells, while the Coulombic efficiency of the NMC||Li_pCC cells stabilizes at a value of ≈99.7% during 100 cycles.

The differences in the cycling behavior become apparent when comparing the individual electrode potential profiles. Although the NMC potential profiles (Figure S4, Supporting Information) look similar for both cells, the overpotentials at the pure Li_p and composite Li_pCC electrodes (Figure 7c,d) differ quite essentially during the Li electrodissolution reaction (i.e., discharge reaction), while the electrochemical behavior of the two electrodes during the charge process is quite similar. In the case of pure Li_p electrodes (Figure 7c), the Li electrodissolution reaction occurs around 0.02 V versus Li/Li^+ followed by an abrupt polarization, indicating an early termination of the electrochemical reaction. Such behavior is observed even in

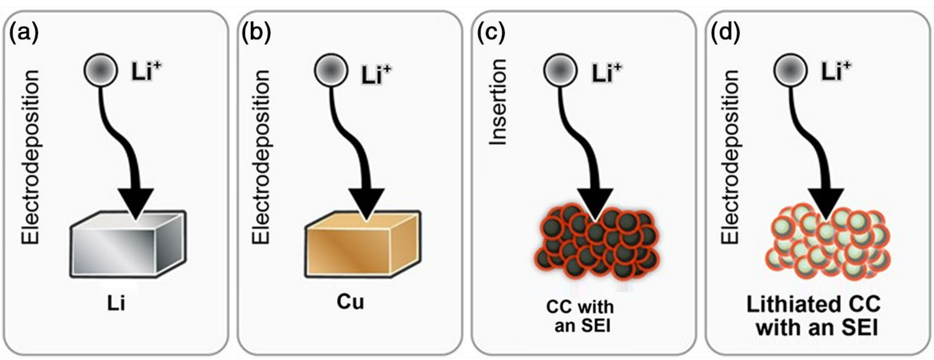

Figure 5. The four charge storage mechanisms in Li_pCC electrodes depicting schematically the Li electrodeposition on a) Li, b) Cu, and c) Li insertion into CC. d) Li electrodeposition on lithiated CC.

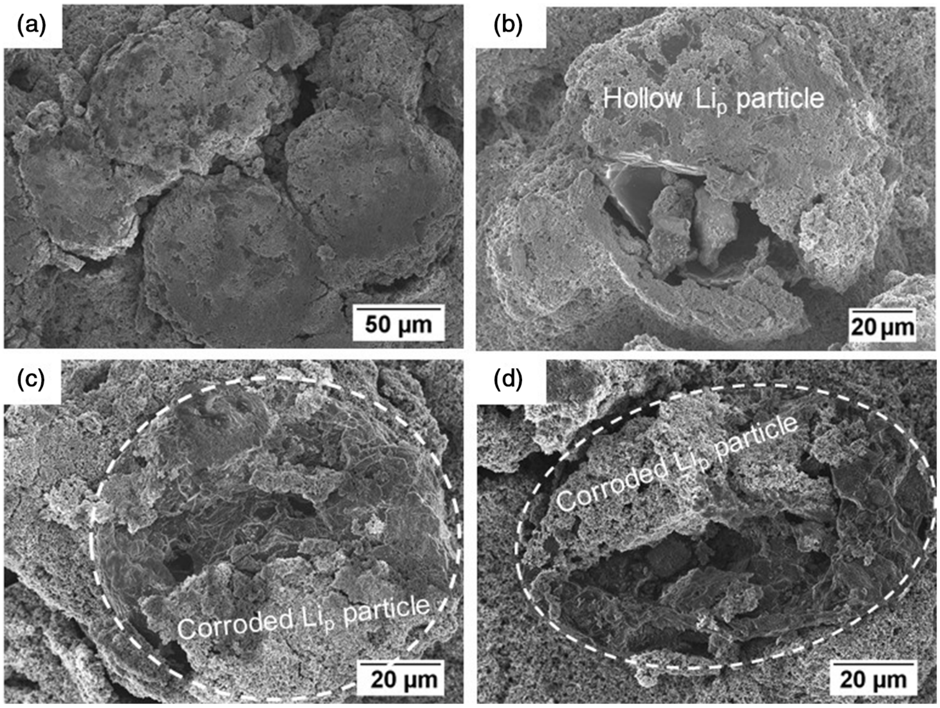

Figure 6. Top-view SEM images of the composite Li_pCC electrode aged for 7 days in a Li||Li symmetric cell (under OCV) assembled with the electrolyte 1 M $LiPF_6$ in EC:DEC 3:7 (w/w). Most of the electrode surface does not reveal any a) morphology changes, probably, due to the reason that it is masked by CC which covers Li_p particles. b–d) Individual Li_p particles demonstrating signs of corrosion were identified. Dashed lines indicate an original shape of corroded Li_p particles.

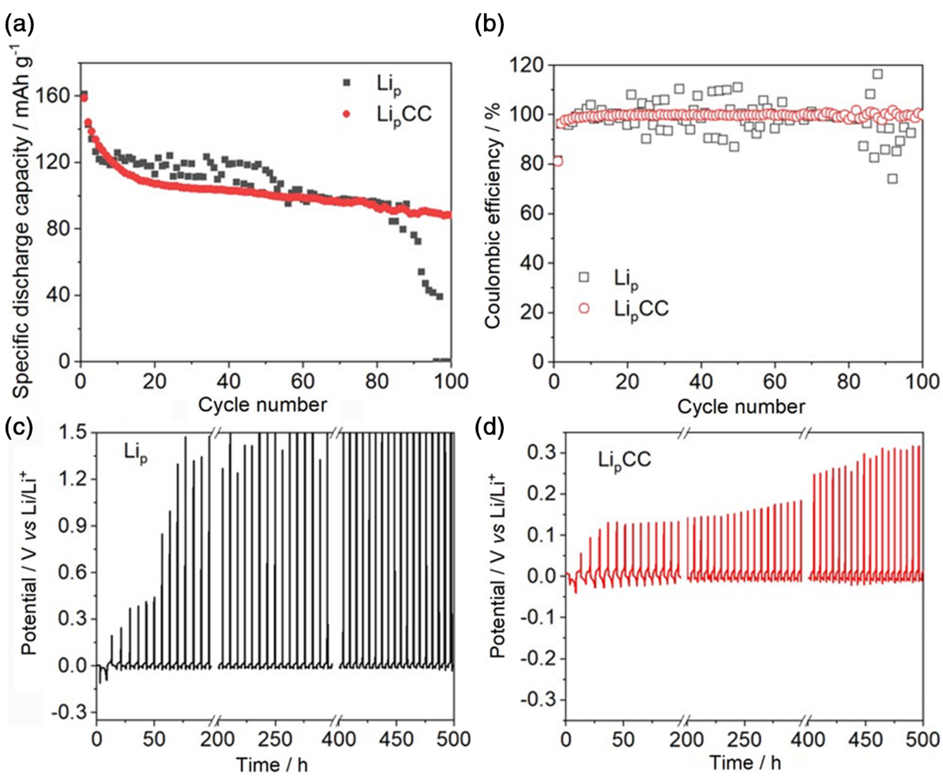

Figure 7. Constant current cycling measurements of Li_p and Li_pCC electrodes in full cells with NMC 622 as cathode, showing a) the specific discharge capacities and the b) corresponding Coulombic efficiencies. The potential profiles of the negative electrodes versus Li/Li^+ for c) pure Li_p electrode and d) composite Li_pCC electrode. The cycling was carried out at a C rate of 0.2C/0.2C for the charge/discharge processes.

the first cycle and continues to accentuate with subsequent cycling, thus suggesting a poor utilization of the active material and also the poor Coulombic efficiency of the Li electrodeposition/electrodissolution process in these electrodes. In contrast, composite Li_pCC electrodes (Figure 7d) clearly demonstrate an improved electrochemical behavior, although the potential of the Li electrodissolution process occurs also around 20 mV versus Li/Li^+. However, during more than 300 h, the increase in the polarization potential indicating the termination of the electrochemical reaction does not increase above a potential value of ≈0.23 V (0.36 V after 600 h). Although the electrodeposition reaction occurs for both electrodes at the same potentials, for the pure Li_p electrode, the Li electrodissolution is more hindered than Li electrodeposition.[5] This can be explained assuming the differences in the electrode bulk composition and thus the resulting areas available for the Li electrodeposition process.

Based on the results and observations previously made, the role of the CC in Li_pCC electrodes can be schematically shown in **Figure 8**.

In this schematic, the effects of the CC can be summarized as follows. 1) An improved electronic contact between the Li_p particles and the Cu current collector, demonstrated in Figure 8a using arrows, is assured due to the high electronic conductivity of CC that results in the higher practical electrode capacity; 2) Due to the high interfacial area between CC and the electrolyte, enhanced SEI formation (demonstrated in Figure 8b by the red circles around CC particles) takes place on the (lithiated) CC surface, which also leads to corrosion and dissolution of the Li_p particles; 3) Reversible Li-ion insertion into CC (Figure 8c); and 4) Li electrodeposition on CC (Figure 8d) result in the lower overvoltage and prolonged cycle life of Li||Li symmetric cells. In this context, the engineering of the surface of the Li_p particles and of the Cu current collector (artificial SEI, selective coatings, etc.) could help to control Li electrodeposition/electrodissolution on pure Li_p electrodes by directing the Li-ion flux in the desired direction.

4. Conclusion

DET was successfully applied for Li_p particle synthesis, which further was used for the preparation of pure Li_p electrodes by an electrode paste-casting method. The HC Li_p electrodes delivered considerably higher practical electrode capacities in comparison with the pure Li_p electrodes (6.3 vs. 1.8 mAh cm^{-2}), that indicates only partial utilization of Li in the pure Li_p electrodes. Application of conductive additives is recommended for Li_p electrodes as the composite Li_pCC electrodes containing 5 wt.% of CC demonstrated enhanced practical electrode capacity in Cu||Li cells up to 3.9 mAh cm^{-2} and better electrochemical performance in NMC||Li cells in comparison with cells based on pure Li_p electrodes. This can be attributed to the enhanced transport of ions and electrons through the aid of lithiated (thus both electronically and ionically) conductive carbon with high interface area to Li_p particles.

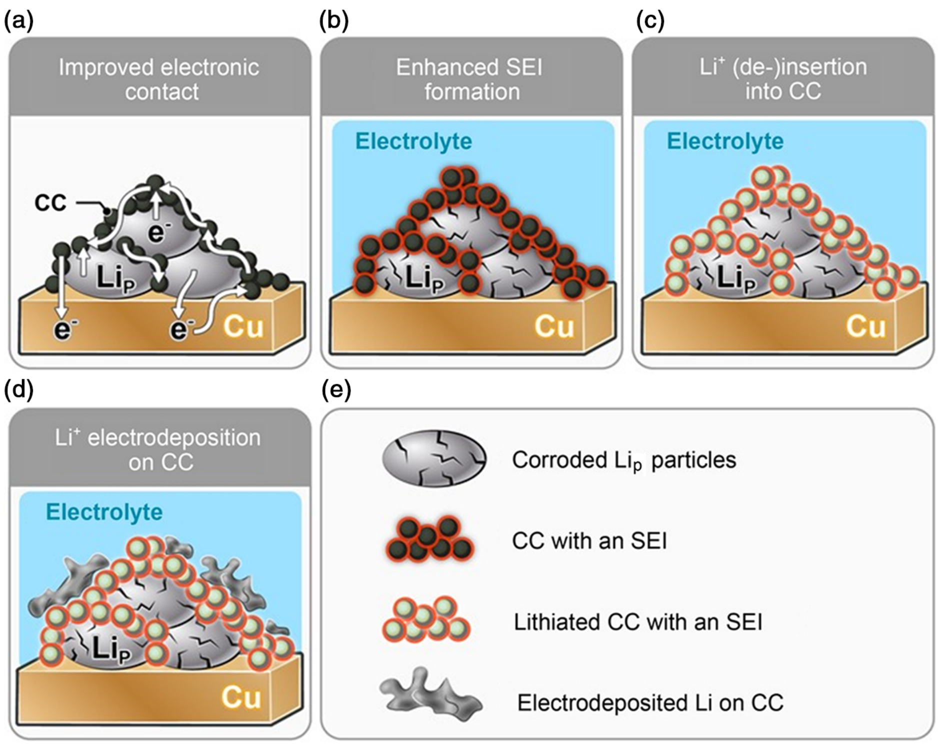

Figure 8. Effects of conductive carbon (CC) in Li_pCC electrodes. a) Improved electronic contact between Li_p particles and Cu current collector results in higher practical electrode capacity. b) Enhanced SEI formation due to a high interface area of CC with an electrolyte results in Li_p corrosion and consumption of the electrochemically active Li. c) Reversible Li^+ insertion into CC and d) Li^+ electrodeposition on CC result in lower overvoltages and prolonged cycling life of Li||Li symmetric cells. e) A common legend for schematic depictions (a–d).

Our results show that the Li electrodissolution from the pure Li_p electrodes remains the most challenging process for such electrodes due to the "dead Li" formation, especially induced by Li electrodissolution near the junction to the current collector. Even though the introduction of an electronically conductive additive that after lithiation contributes to the electronic and ionic conductivity within the bulk of the powder-based electrodes, further measures have to be considered to enhance the practical capacities of such electrodes. In fact, in the shown experiments, quick consumption of electrochemically active Li causes an increase in the electrode potential leading to premature cell failure.

Supporting Information

Supporting Information is available from the Wiley Online Library or from the author.

Acknowledgements

The authors acknowledge the German Federal Ministry of Education and Research (BMBF) for the financial support within the projects BCT-Battery Cell Technology (03XP0109I) and MEET Hi-EnD III - Materials and Components to Meet High Energy Density Batteries (03XP0258A). The authors would like to acknowledge Andre Bar for the support with the graphical figures within this manuscript. The authors are also grateful for the efforts of Vladislav Mayer, Sven Eppenhoff and the team of the mechanical workshop (WWU Muenster, Institute of Physics) in designing and manufacturing the apparatus for the Li_p synthesis.

Open access funding enabled and organized by Projekt DEAL.

Conflict of Interest

The authors declare no conflict of interest.

Data Availability Statement

Research data are not shared.

Keywords

droplet emulsion technique, electrodeposition, electrodissolution, lithium metal batteries, lithium powder-based electrodes

Received: September 29, 2021
Revised: October 27, 2021
Published online: December 4, 2021

[1] T. Placke, R. Kloepsch, S. Dühnen, M. Winter, *J. Solid State Electrochem.* **2017**, *21*, 1939.
[2] G. E. Blomgren, *J. Electrochem. Soc.* **2016**, *164*, A5019.
[3] S. Dühnen, J. Betz, M. Kolek, R. Schmuch, M. Winter, T. Placke, *Small Methods* **2020**, *4*, 2000039.
[4] D. Jin, J. Park, M. H. Ryou, Y. M. Lee, *Adv. Mater. Interfaces* **2020**, *7*, 1902113.
[5] G. Bieker, M. Winter, P. Bieker, *Phys. Chem. Chem. Phys.* **2015**, *17*, 8670.
[6] M. H. Ryou, Y. M. Lee, Y. Lee, M. Winter, P. Bieker, *Adv. Funct. Mater.* **2015**, *25*, 834.
[7] M. C. Stan, J. Becking, A. Kolesnikov, B. Wankmiller, J. E. Frerichs, M. R. Hansen, P. Bieker, M. Kolek, M. Winter, *Mater. Today* **2020**, *39*, 137.
[8] R. Mogi, M. Inaba, S.-K. Jeong, Y. Iriyama, T. Abe, Z. Ogumi, *J. Electrochem. Soc.* **2002**, *149*, A1578.
[9] J. Chen, J. Zhao, L. Lei, P. Li, J. Chen, Y. Zhang, Y. Wang, Y. Ma, D. Wang, *Nano Lett.* **2020**, *20*, 3403.
[10] P. Zhai, Y. Wei, J. Xiao, W. Liu, J. Zuo, X. Gu, W. Yang, S. Cui, B. Li, S. Yang, *Adv. Energy Mater.* **2020**, *10*, 1903339.
[11] C. Y. Fan, D. Xie, X. H. Zhang, W. Y. Diao, R. Jiang, X. L. Wu, *Adv. Funct. Mater.* **2021**, *31*, 2102158.
[12] Y. Han, B. Liu, Z. Xiao, W. Zhang, X. Wang, G. Pan, Y. Xia, X. Xia, J. Tu, *InfoMat* **2021**, *3*, 155.
[13] J. Besenhard, J. Yang, M. Winter, *J. Power Sources* **1997**, *68*, 87.
[14] M. Wan, S. Kang, L. Wang, H.-W. Lee, G. W. Zheng, Y. Cui, Y. Sun, *Nat. Commun.* **2020**, *11*, 829.
[15] M. Winter, J. Besenhard, J. Albering, J. Yang, M. Wachtler, *Prog. Batteries Battery Mater.* **1998**, *17*, 208.
[16] D. Xie, H.-H. Li, W.-Y. Diao, R. Jiang, F.-Y. Tao, H.-Z. Sun, X.-L. Wu, J.-P. Zhang, *Energy Storage Mater.* **2021**, *36*, 504.
[17] J. Heine, P. Hilbig, X. Qi, P. Niehoff, M. Winter, P. Bieker, *J. Electrochem. Soc.* **2015**, *162*, A1094.
[18] J. Qian, W. A. Henderson, W. Xu, P. Bhattacharya, M. Engelhard, O. Borodin, J.-G. Zhang, *Nat. Commun.* **2015**, *6*, 6362.
[19] J. R. Nair, L. Imholt, G. Brunklaus, M. Winter, *Electrochem. Soc. Interface* **2019**, *28*, 55.
[20] S. Randau, D. A. Weber, O. Kötz, R. Koerver, P. Braun, A. Weber, E. Ivers-Tiffée, T. Adermann, J. Kulisch, W. G. Zeier, *Nat. Energy* **2020**, *5*, 259.
[21] S. W. Kim, Y. J. Ahn, W. Y. Yoon, *Metals Mater.* **2000**, *6*, 345.
[22] M. Winter, *Z. Phys. Chem.* **2009**, *223*, 1395.
[23] B. M. Song, H. E. Park, W. Yoon, B. K. Kim, *J. Korean Phys. Soc.* **2009**, *54*, 1136.
[24] D. Jin, J. Oh, A. Friesen, K. Kim, T. Jo, Y. M. Lee, M.-H. Ryou, *ACS Appl. Mater. Interfaces* **2018**, *10*, 16521.
[25] S. W. Hwang, J. H. Yom, S. M. Cho, W. Y. Yoon, *ACS Appl. Mater. Interfaces* **2017**, *9*, 22530.
[26] A. Kolesnikov, D. Zhou, M. Kolek, J. P. B. Jimenez, P. Bieker, M. Winter, M. C. Stan, *J. Electrochem. Soc.* **2019**, *166*, A1400.
[27] J.-A. Choi, J.-H. Yoo, W. Y. Yoon, D.-W. Kim, *Electrochim. Acta* **2014**, *132*, 1.
[28] S.-T. Hong, J.-S. Kim, S.-J. Lim, W. Y. Yoon, *Electrochim. Acta* **2004**, *50*, 535.
[29] A. Kolesnikov, M. Kolek, J. F. Dohmann, F. Horsthemke, M. Börner, P. Bieker, M. Winter, M. C. Stan, *Adv. Energy Mater.* **2020**, *10*, 2000017.
[30] C. M. Long, M. A. Nascarella, P. A. Valberg, *Environ. Pollut.* **2013**, *181*, 271.
[31] C.-C. Li, Y.-S. Lin, *J. Power Sources* **2012**, *220*, 413.
[32] S. K. Martha, H. Sclar, Z. S. Framowitz, D. Kovacheva, N. Saliyski, Y. Gofer, P. Sharon, E. Golik, B. Markovsky, D. Aurbach, *J. Power Sources* **2009**, *189*, 248.
[33] X. Qi, B. Blizanac, A. DuPasquier, A. Lal, P. Niehoff, T. Placke, M. Oljaca, J. Li, M. Winter, *J. Electrochem. Soc.* **2014**, *162*, A339.
[34] X. Qi, B. Blizanac, A. DuPasquier, P. Meister, T. Placke, M. Oljaca, J. Li, M. Winter, *Phys. Chem. Chem. Phys.* **2014**, *16*, 25306.
[35] X. Qi, B. Blizanac, A. DuPasquier, M. Oljaca, J. Li, M. Winter, *Carbon* **2013**, *64*, 334.
[36] K. Pfeifer, S. Arnold, Ö. Budak, X. Luo, V. Presser, H. Ehrenberg, S. Dsoke, *J. Mater. Chem. A* **2020**, *8*, 6092.
[37] R. Nölle, K. Beltrop, F. Holtstiege, J. Kasnatscheew, T. Placke, M. Winter, *Mater. Today* **2020**, *32*, 131.

[38] H. Mollet, A. Grubenmann, *Formulation Technology: Emulsions, Suspensions, Solid Forms*, WILEY-VCH Verlag GmbH, Weinheim **2001**.
[39] T. F. Tadros, *Emulsion Formation, Stability, and Rheology*, Wiley-VCH Verlag GmbH, Weinheim **2013**.
[40] L. L. Schramm, *Emulsions, Foams, Suspensions, and Aerosols: Microscience and Applications*, John Wiley & Sons, Hoboken, NJ **2014**.
[41] M. Jaszczur, A. Młynarczykowska, L. Demurtas, *Energies* **2020**, *13*, 640.
[42] J. N. Nayak, M. I. Aralaguppi, U. S. Toti, T. M. Aminabhavi, *J. Chem. Eng. Data* **2003**, *48*, 1483.
[43] C. Franjo, L. Segade, C. Menaut, J. Pico, E. Jiménez, *J. Solution Chem.* **2001**, *30*, 995.
[44] P. Zou, Y. Wang, S.-W. Chiang, X. Wang, F. Kang, C. Yang, *Nat. Commun.* **2018**, *9*, 1.
[45] Z. Lu, Q. Liang, B. Wang, Y. Tao, Y. Zhao, W. Lv, D. Liu, C. Zhang, Z. Weng, J. Liang, *Adv. Energy Mater.* **2019**, *9*, 1803186.
[46] F. Ding, W. Xu, G. L. Graff, J. Zhang, M. L. Sushko, X. Chen, Y. Shao, M. H. Engelhard, Z. Nie, J. Xiao, *J. Am. Chem. Soc.* **2013**, *135*, 4450.
[47] C.-P. Yang, Y.-X. Yin, S.-F. Zhang, N.-W. Li, Y.-G. Guo, *Nat. Commun.* **2015**, *6*, 1.
[48] J. B. Goodenough, *J. Solid State Electrochem.* **2012**, *16*, 2019.
[49] V. A. Sethuraman, L. J. Hardwick, V. Srinivasan, R. Kostecki, *J. Power Sources* **2010**, *195*, 3655.
[50] D. Lin, Y. Liu, Y. Li, Y. Li, A. Pei, J. Xie, W. Huang, Y. Cui, *Nat. Chem.* **2019**, *11*, 382.
[51] J. F. Dohmann, F. Horsthemke, V. Küpers, S. Bloch, Y. Preibisch, A. Kolesnikov, M. Kolek, M. C. Stan, M. Winter, P. Bieker, *Adv. Energy Mater.* **2021**, *11*, 2101021.
[52] F. Holtstiege, A. Wilken, M. Winter, T. Placke, *Phys. Chem. Chem. Phys.* **2017**, *19*, 25905.

